

See discussions, stats, and author profiles for this publication at: <https://www.researchgate.net/publication/362812760>

Mutualistic Cooperative Ambient Backscatter Communications Under Hardware Impairments

Article in IEEE Transactions on Communications · August 2022

DOI: 10.1109/TCOMM.2022.3201119

CITATIONS

49

READS

86

5 authors, including:



Yinghui Ye

Xi'an University of Posts and Telecommunications

140 PUBLICATIONS 2,404 CITATIONS

SEE PROFILE



Liqin Shi

Xi'an University of Posts and Telecommunications

67 PUBLICATIONS 1,319 CITATIONS

SEE PROFILE



Xiaoli Chu

The University of Sheffield

307 PUBLICATIONS 9,999 CITATIONS

SEE PROFILE

Mutualistic Cooperative Ambient Backscatter Communications under Hardware Impairments

Yinghui Ye, Liqin Shi, Xiaoli Chu, *Senior Member, IEEE*, Guangyue Lu, and
Sumei Sun, *Fellow, IEEE*

Abstract

Mutualistic cooperative ambient backscatter communications (AmBC) have been proposed to improve the spectrum and energy efficiencies of Internet-of-Things (IoT) systems, where a primary link (from a primary transmitter to a primary receiver) and an AmBC link (from an IoT device to the same primary receiver) form a mutualism relationship. We note that hardware impairments (HIs), which are unavoidable in practical systems and may significantly affect the transmission rates of the primary and AmBC links and their mutualism relationships, have been largely ignored in the study of mutualistic cooperative AmBC networks. In this paper, we study a mutualistic cooperative AmBC network with HIs at all the active transceivers and a non-linear energy harvesting circuit at each IoT device. We derive closed-form rate expressions for both the AmBC and primary links and theoretically prove that the mutualism relationship between the AmBC and primary links is maintained under HIs, i.e., the rate of the primary link in the mutualistic cooperative AmBC network is still higher than that without the AmBC link. To maximize the weighted sum rate of all links in a cooperative AmBC network under HIs, we propose two resource allocation schemes for two scenarios with a single link and multiple AmBC links, respectively. For the single AmBC link case, we derive the optimal transmit power of the primary transmitter and the optimal power reflection coefficient of the IoT device in closed forms. For the scenario with multiple AmBC links, the weighted-sum-rate maximization problem is transformed into

Part of this work has been accepted by the IEEE ICC [1]. Yinghui Ye, Liqin Shi and Guangyue Lu are with the Shaanxi Key Laboratory of Information Communication Network and Security, Xi'an University of Posts & Telecommunications, China (connecttyh@126.com, liqinshi@hotmail.com, tonylgy@163.com). Xiaoli Chu is with the Department of Electronic and Electrical Engineering, The University of Sheffield, U.K. (e-mail: x.chu@sheffield.ac.uk). Sumei Sun is with the Institute of Infocomm Research, Agency for Science, Technology and Research, Singapore. (e-mail: sunsm@i2r.a-star.edu.sg)

a convex one and solved with convex optimization tools. Computer simulations validate our theoretical results and that our proposed schemes outperform the benchmark schemes in terms of the weighted sum rate.

Index Terms

Ambient backscatter communications, hardware impairment, mutualism relationship, resource allocation.

I. INTRODUCTION

LARGE-SCALE Internet-of-Things (IoT) deployments are facing challenges due to the limited battery capacity of devices and scarce spectrum resources. Ambient backscatter communications (AmBC) have been proposed as a spectrum- and energy-efficient solution for IoT [1]–[4]. The basic principle of AmBC is to allow an IoT device to adjust its the antenna's load impedance to passively modulate information on the incident signals and backscatter the modulated signals to the associated receiver, while harvesting energy from the incident signals to support its circuit operation [3], [4]. AmBC has been validated by various practical prototypes [5]–[7]. The transmission rate of an AmBC link is limited by the co-channel interference, because the AmBC receiver receives both the primary transmitter's (PT's) and AmBC transmitter's¹ signals simultaneously and the PT's signal is usually much stronger than that of AmBC. Meanwhile, due to the non-cooperative spectrum sharing between the primary link and the AmBC link, it is hard for the AmBC receiver to obtain the channel state information of each link, hence cannot remove the severe co-channel interference caused by the PT's signal [8]. To address this problem, one way is to enable certain forms of cooperation at the AmBC receiver to remove the co-channel interference from the PT by designing sophisticated symbol detectors [9], [10]. Another way to overcome the above challenge is to design novel cooperative AmBC [11], [12], where the primary link and the AmBC link are jointly designed to remove or suppress the co-channel interference. Depending on whether the AmBC modulation rate is equal to or much slower than that of PT, cooperative AmBC can be classified into parasitic cooperative AmBC

¹In this paper, the AmBC transmitter and the IoT device are interchangeably used.

and mutualistic cooperative AmBC. In the former, the AmBC receiver firstly decodes the PT's signal while treating the interference from the AmBC link as noise and then removes the decoded PT signal from the composite received signal to decode the AmBC signal [13]. In the latter, as the AmBC modulation rate is much slower than that of the PT and the received AmBC signal includes both the PT's and the IoT device's information, the AmBC link can provide an additional multipath gain for the primary receiver to decode the PT's signal, forming a mutualism relationship between the primary and AmBC links [11], [14], [15].

In [15], the authors maximized the weighted sum rate of both the primary and AmBC links by jointly optimizing the PT's transmit power and beamforming vectors in parasitic and mutualistic cooperative AmBC networks, respectively. The similar optimizations were also studied in [16] by considering the finite block length in AmBC links. The authors of [17] formulated a stochastic optimization to maximize the utility function of the signal-to-interference-plus-noise ratio (SINR) by jointly optimizing the PT's transmit beamforming and its associated receiver's beamforming. In [18], the authors considered a parasitic cooperative AmBC network with a full-duplex IoT device, where the IoT device splits the incident signal into two parts for message decoding and passive transmission simultaneously, and the PT's transmit power was minimized by jointly optimizing the PT's beamforming vectors and the IoT device's power splitting ratio. Considering the energy-causality constraint at each IoT device, the authors in [19] jointly optimized the PT's transmit power and the IoT device's power reflection coefficient and backscattering time to maximize the energy efficiency in parasitic and mutualistic cooperative AmBC networks, respectively. In addition to the above works [15]–[19] with a focus on resource allocation, performance evaluation was also studied in cooperative AmBC networks. In [20], the outage probability and the diversity gain of a parasitic cooperative AmBC network were derived. Combining parasitic cooperative AmBC with downlink non-orthogonal multiple access (NOMA), the outage probability and the ergodic capacity were analyzed theoretically in [21]. Considering a mutualistic cooperative AmBC network, the authors in [22] derived the upper bounds of the ergodic capacity for both the primary and AmBC links.

In the above works [15]–[22], the radio frequency (RF) front ends of each transceiver are assumed to be ideal, and it has been shown that the AmBC link can offer beneficial multipath

diversity to the primary link and thus the primary link achieves a higher transmission rate than the case without the AmBC link, i.e., there is a mutualism relationship between the primary and AmBC links [15]. Nevertheless, in practical communications, RF front ends are susceptible to a variety of hardware impairments (HIs), e.g., in-phase/quadrature imbalance, quantization error, etc [23]–[25]. The HIs will distort the signals generated by the transmitter and thus degrade the information decoding performance at the receiver. In spite of the efforts on the development of mitigation algorithms, there always exist residual HIs due to the time-varying hardware characteristics. Although in a very recent work [26], the authors derived the expressions for both the outage probability and intercept probability in a *parasitic* cooperative NOMA-AmBC network, where the RF front ends of all transceivers suffer HIs, the impacts of HIs on the *mutualistic* cooperative AmBC network are still unknown. In the presence of HIs, the AmBC link not only brings an additional multipath diversity gain but also backscatters the distortion noises caused by HIs at the PT's front ends to the primary link. In this regard, the following question arises: does the mutualism relationship between the primary and AmBC links still exist in the presence of HIs? Moreover, the resource allocation for cooperative AmBC networks under HIs has not been studied.

In this work, we study the impact of HIs on a *mutualistic* cooperative AmBC network, where an IoT device modulates its information on the incident signal transmitted by the PT with a much slower symbol rate than that of PT while harvesting energy from the PT's signal for sustaining its operation, and design resource allocation schemes to maximize the weighted sum rate of the primary and AmBC links under HIs. A non-linear energy harvesting model is considered for each IoT device as it better reflects the non-linear properties of energy harvesting circuits. The main contributions are summarized as follows.

- We theoretically prove the following three results to reveal the impacts of HIs on the achievable rates of the primary link and the AmBC link. First, the rate of each link under HIs is strictly lower than that without HIs. Second, under given HIs, the primary link's rate in the considered mutualistic cooperative AmBC network is strictly higher than that without any spectrum-sharing AmBC link. Third, the HIs lead to the rate ceilings for the primary and AmBC links. The first two results validate that the existence of HIs degrades the rate of

both the AmBC and primary links but does not destroy the mutualism relationship between them. Compared with [15], our conclusion² is more rigorous and the details are summarized in Remark 2. In the third result, we derive the upper-bound rate of the primary link and that of the AmBC link at a very high transmit power of the PT. Besides, we derive a closed-form expression of the primary link's rate under the assumption that the modulated information of the IoT device follows a symmetric complex Gaussian distribution.

- We design resource allocation schemes to maximize the weighted sum rate in mutualistic cooperative AmBC networks with a single AmBC link or multiple AmBC links, while considering HIs. For the case with a single AmBC link, we derive the optimal power reflection coefficient of the IoT device and the optimal transmit power of the PT that maximize the weighted sum rate of the primary and AmBC links, subject to the energy-causality constraint of the IoT device. For the case with multiple AmBC links, we formulate a non-convex problem to maximize the weighted sum rate of all links by jointly optimizing the power reflection coefficient and backscattering time of each IoT device and the transmit power of the PT. By exploiting the monotonicity of the primary link's rate and the AmBC link's rate and constructing auxiliary variables, the original problem is transformed into a more tractable form, the convexity of which depends on the energy harvesting model considered for each IoT device. By introducing a non-linear but convex energy harvesting model, the transformed problem is shown to be convex and solved by the convex tools.

The rest of the paper is organized as follows. In Section II, the system model and the rate of the primary and AmBC links under HIs are presented. Section III studies the impacts of HIs on the mutualism relationship between the primary and AmBC links, and derives the closed-form rate expressions for both the primary and AmBC links. In Section IV, two resource allocation schemes are developed to maximize the weighted sum rate. Simulation results are provided in Section V and Section VI draws the main conclusion.

²The ideal hardware in [15] is a special case of our considered model, thus the conclusion that the mutualism relationship between the AmBC and primary link exists is also valid for the ideal case.

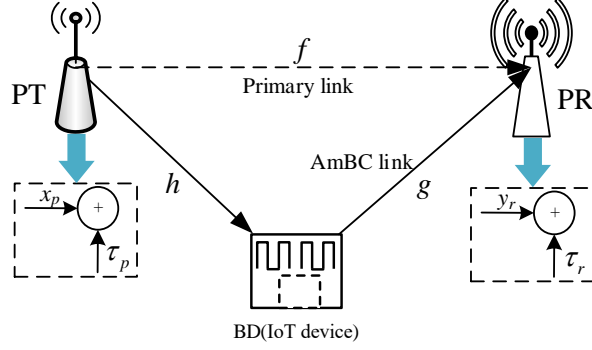


Fig. 1. Mutualistic cooperative AmBC network with a single AmBC link.

II. SYSTEM MODEL AND RATE ANALYSIS

In this section, we first introduce the system model and the associated assumptions, and then analyze the rate of the primary and AmBC links in the presence of HIs.

A. System Model and Assumption

Fig. 1 shows a mutualistic cooperative AmBC network that consists of one PT, one primary receiver (PR), and one IoT device (also referred to as a backscatter device (BD) hereafter). Both PT and PR are non-energy-constrained transceivers that are composed of active components, e.g., oscillators, analog-to-digital/digital-to-analog converters. Each BD consists of a backscatter circuit and an energy harvesting circuit. The channel power gains of the PT-BD link, the PT-PR link (also termed as the primary link), and the BD-PR link (also termed as the AmBC link) are denoted by h , f , g , respectively. A block-fading channel model is considered, i.e., all the channel power gains stay constant within each transmission block but may change across different transmission blocks. To obtain the performance bound of both primary and AmBC links, we assume perfect channel state information (CSI) and the details on how to obtain CSI can be found in [3] and [15]. Relaxing this assumption makes our considered network close to practical scenarios, which is a new challenge and can be studied in the future.

Let $x_p(n)$ and $c_s(i)$ denote the primary signal in the n -th symbol period and the AmBC signal in the i -th symbol period, respectively. Due to the simple backscatter circuit in the BD and the low modulation rate of the BD, the symbol period of $x_p(n)$, denoted by T_p , is shorter than that

of $c_s(i)$, denoted by T_c . For analytical tractability, we assume that $T_c = LT_p$, where $L \gg 1$ is a positive integer, and that $x_p(n)$ follows an independent circularly symmetric complex Gaussian distribution, i.e., $x_p(n) \sim \mathcal{CN}(0, 1)$. Also, the mean and variance of $c_s(i)$ are assumed to be zero and one, respectively.

B. Rate Analysis Considering HIs

In the considered network, PT and BD work in the cooperative mode and transmit their information to the PR by sharing the same resource block. More specifically, BD modulates its own information on the incident signal transmitted by the PT and reflects the modulated signal to the PR, while harvesting energy to sustain its backscatter operation by varying the power reflection coefficient β . Accordingly, the signal transmitted by the PT and the incident signal arriving at the BD can be written as, respectively³,

$$y_{\text{PT}}(n) = x_p(n) + \tau_p(n), \quad (1)$$

$$y_{\text{BD}}(n) = \sqrt{h}(x_p(n) + \tau_p(n)), \quad (2)$$

where $\tau_p(n)$ is the distortion noise caused by HIs of the PT. $\tau_p(n)$ follows an independent zero-mean circularly symmetric complex Gaussian distribution, and its variance is the product of the average power of the PT's signal P_0 and the square of HI level parameter κ_p [24], i.e., $\tau_p(n) \sim \mathcal{CN}(0, \kappa_p^2 P_0)$.

Through a power reflection coefficient β , the received signal $y_{\text{BD}}(n)$ is split into two parts: one is used as the carrier for modulating and backscattering information⁴ $c_s(i)$ to the PR, while the other is harvested for powering its backscatter circuit. Accordingly, the received signal of the PR and the harvested power of the BD can be expressed as, respectively,

$$y_{\text{PR}}(n) = \underbrace{\sqrt{\beta h g}(x_p(n) + \tau_p(n)) c_s(i)}_{\text{PT} \rightarrow \text{BD} \rightarrow \text{PR link}} + \underbrace{\sqrt{f}(x_p(n) + \tau_p(n))}_{\text{PT} \rightarrow \text{PR link}} + \tau_r(n) + w(n), \quad (3)$$

³Similar to [8], [11]–[13], [27], here we omit the thermal noise at the BD as its power introduced by the passive components is much smaller than that of $h(x_p(n) + \tau_p(n))$.

⁴The BD adjusts its antenna's load impedance to passively modulate information $c_s(i)$ on the incident signal $y_{\text{BD}}(n)$ and backscatter the modulated signal to the PR [3], which avoids the imperfect RF components. Thus, there is no distortion noise introduced by the BD.

$$E_{\text{BD}} = \varphi \left((1 - \beta) h P_0 (1 + \kappa_p^2) \right), \quad (4)$$

where $w(n)$ is the additive complex white Gaussian noise with mean zero and variance σ^2 , $\varphi(\cdot)$ is a non-decreasing function to reflect the relationship between the input power and the harvested power for a practical energy harvester, $\tau_r(n)$ is the hardware distortion noise, and follows the Gaussian distribution with a zero mean and a variance that equals the product of the average power of the incident signal and the square of the HI level parameter κ_r [24]. For given $c_s(i)$, the average power of the incident signal in a symbol period is given by $P_0 (1 + \kappa_p^2) (h\beta g |c_s(i)|^2 + f)$, while the average power of the incident signal in a transmission block, which is much longer than a symbol period of the BD, is given by $P_0 (1 + \kappa_p^2) (h\beta g \mathbb{E}[|c_s(i)|^2] + f) = \kappa_r^2 P_0 (1 + \kappa_p^2) (h\beta g + f)$, where $\mathbb{E}[|c_s(i)|^2] = 1$. Accordingly, the distribution of $\tau_r(n)$ can be written as

$$\tau_r(n) \sim \begin{cases} \mathcal{CN}(0, \kappa_r^2 P_0 (1 + \kappa_p^2) (h\beta g |c_s(i)|^2 + f)), & \text{within one BD symbol period} \\ \mathcal{CN}(0, \kappa_r^2 P_0 (1 + \kappa_p^2) (h\beta g + f)), & \text{within one transmission block} \end{cases}. \quad (5)$$

As $T_c = LT_p$, $c_s(i)$ spans L primary symbol periods for $n = 1, 2, \dots, L$, i.e., $c_s(i)$ keeps almost unchanged for decoding $x_p(n)$, $n = 1, 2, \dots, L$. For a given $c_s(i)$, the first term in (3) can be rewritten as $\sqrt{\beta h g} x_p(n) c_s(i) + \sqrt{\beta h g} \tau_p(n) c_s(i)$, where $\sqrt{\beta h g} x_p(n) c_s(i)$ and $\sqrt{\beta h g} \tau_p(n) c_s(i)$ can be regarded as the output of the PT signal $x_p(n)$ passing through a slowly varying channel $\sqrt{\beta h g} c_s(i)$ and the Gaussian noise with variance $\kappa_p^2 P_0 \beta h g |c_s(i)|^2$. Accordingly, the SINR to decode $x_p(n)$ and the achievable rate of $x_p(n)$ within the symbol period of $c_s(i)$ can be calculated as, respectively,

$$\gamma_{x_p}(c_s(i)) = \frac{P_0 h \beta g |c_s(i)|^2 + P_0 f}{P_0 (h \beta g |c_s(i)|^2 + f) \kappa + \sigma^2}, \quad (6)$$

$$R_p(c_s(i)) = B_w \log_2 (1 + \gamma_{x_p}(c_s(i))), \quad (7)$$

where B_w denotes the communication bandwidth, and $\kappa = \kappa_r^2 \kappa_p^2 + \kappa_r^2 + \kappa_p^2$.

By assuming that the number of symbols of the BD signal is sufficiently large within one transmission block, then the average rate of $x_p(n)$ within one transmission block can be derived as

$$\mathcal{C}_p = \mathbb{E}_{c_s(i)} [R_p(c_s(i))], \quad (8)$$

where $\mathbb{E}_x[\cdot]$ denotes the expectation operator over the random variable x .

After obtaining the rate of the primary link, we derive the rate of the AmBC link. We assume for simplicity that $\sqrt{hf}x_p(n)$ can be perfectly removed from $y_{\text{PR}}(n)$ via successive interference cancellation (SIC). Thus, the remaining signal at the PR to decode $c_s(i)$ is given by

$$\hat{y}_{\text{PR}}(n) = \sqrt{\beta hg}(x_p(n) + \tau_p(n))c_s(i) + \sqrt{f}\tau_r(n) + \tau_r(n) + w(n). \quad (9)$$

As the average power of $x_p(n)$ equals one and one BD symbol, e.g., $c_s(i)$, is modulated into the L consecutive PT symbol periods, $x_p(n)$, $n = 1, 2, \dots, L$, the maximal ratio combining (MRC) can be performed on $\hat{y}_{\text{PR}}(n)$, $n = 1, 2, \dots, L$, which are received in L consecutive primary symbol periods, to decode $c_s(i)$. The resulting average SINR can be calculated as

$$\begin{aligned} \gamma_{c_s} &= \sum_{n=1}^L \mathbb{E} \left[\frac{\beta hg |x_p(n)|^2}{|\tau_p(n)|^2 (\beta hg + f) + |\tau_r(n)|^2 + |w(n)|^2} \right] \\ &= \frac{L\beta hg P_0}{P_0 (\beta hg + f) \kappa + \sigma^2}, \end{aligned} \quad (10)$$

where the second equality holds due to $\mathbb{E}[|x_p(1)|^2] = \mathbb{E}[|x_p(2)|^2] = \dots = \mathbb{E}[|x_p(n)|^2] = P_0$, $\mathbb{E}[|\tau_p(1)|^2] = \mathbb{E}[|\tau_p(2)|^2] = \dots = \mathbb{E}[|\tau_p(n)|^2] = \kappa_p^2 P_0$, $\mathbb{E}[|\tau_r(1)|^2] = \mathbb{E}[|\tau_r(2)|^2] = \dots = \mathbb{E}[|\tau_r(n)|^2] = \kappa_r^2 P_0 (1 + \kappa_p^2) (h\beta g + f)$, and $\mathbb{E}[|w(1)|^2] = \mathbb{E}[|w(2)|^2] = \dots = \mathbb{E}[|w(n)|^2] = \sigma^2$.

In the mutualistic cooperative AmBC network, as modulating one BD symbol requires L consecutive PT symbols, the PT's signal $x_p(n)$ can be viewed as a spread-spectrum code with length L for BD symbols. Accordingly, the SINR to decode $c_s(i)$ is increased by L times at the price of symbol rate decreased by $\frac{1}{L}$, and the BD's rate can be expressed as

$$\mathcal{C}_s = \frac{B_w}{L} \log_2 (1 + \gamma_{c_s}). \quad (11)$$

III. IMPACTS OF HIS

In this section, we study the impacts of HIs on the mutualism relationship between the primary and AmBC links. Besides, we derive the primary link's rate (8) into a closed form.

The rates for the primary link and the AmBC link with ideal hardware can be obtained by substituting $\kappa_p = \kappa_r = 0$ into (8) and (11), i.e.,

$$\mathcal{C}_p^{\text{id}} = \mathbb{E}_{c_s(i)} \left[B_w \log_2 \left(1 + \frac{P_0 h \beta g |c_s(i)|^2 + P_0 f}{\sigma^2} \right) \right], \quad (12)$$

$$\mathcal{C}_s^{\text{id}} = \frac{B_w}{L} \log_2 \left(1 + \frac{LP_0\beta hg}{\sigma^2} \right). \quad (13)$$

Comparing the rates in (12) and (13) with the HIs case in (8) and (11), it is clear that the rates with HIs are strictly lower than those of ideal hardware due to the existence of hardware distortion noises in both the primary and AmBC links, i.e., $\mathcal{C}_p^{\text{id}} > \mathcal{C}_p$ and $\mathcal{R}_s^{\text{id}} > \mathcal{R}_s$ always hold. This indicates that HIs degrade the achievable rates of both the primary and AmBC links. Besides, by assuming $P_0 \rightarrow \infty$ in the case of HIs, we have the following inequality associated with the PT link's rate, i.e.,

$$\mathcal{C}_p \leq B_w \log_2 \left(1 + \frac{h\beta g \mathbb{E}[|c_s(i)|^2] + f}{(h\beta g \mathbb{E}[|c_s(i)|^2] + f)\kappa + \frac{\sigma^2}{P_0}} \right) < B_w \log_2 \left(1 + \frac{1}{\kappa} \right), \quad (14)$$

where the first inequality holds for the Jensen's inequality, and second inequality is derived from that $\frac{h\beta g \mathbb{E}[|c_s(i)|^2] + f}{(h\beta g \mathbb{E}[|c_s(i)|^2] + f)\kappa + \frac{\sigma^2}{P_0}}$ is an increasing function with respect to P_0 and that $\frac{\sigma^2}{P_0}$ approaches to zero as $P_0 \rightarrow \infty$.

Similarly, we can obtain the following inequality on the BD's rate as $P_0 \rightarrow \infty$, given by

$$\mathcal{C}_s < \frac{B_w}{L} \log_2 \left(1 + \frac{L\beta hg}{(\beta hg + f)\kappa} \right). \quad (15)$$

Remark 1. Both (14) and (15) show that the HI levels, i.e., κ_p , κ_r , have significant impacts on the achievable rate. It can be seen that in the case of HIs, the achievable rates of both the primary and AmBC links are bounded at $P_0 \rightarrow \infty$, i.e., there exist rate ceilings for both the primary and AmBC links. Interestingly, the upper bound of \mathcal{C}_p only depends on the HIs, while for the AmBC link, its upper bound is jointly affected by the HIs and the channel power gains. Particularly, the upper bound of \mathcal{C}_s increases with the decrease of f , indicating that a poor channel condition of the PT-PR link raises the ceiling of the AmBC link rate.

To answer the question raised in the Introduction section, we provide the following theorem.

Theorem 1. For given κ_p , κ_r and channel power gains, we have the following inequality, i.e.,

$$\mathcal{C}_p > B_w \log_2 \left(1 + \frac{P_0 f}{P_0 f \kappa + \sigma^2} \right), \quad (16)$$

where \mathcal{C}_p denotes the achievable rate of the primary link with ideal hardware, and the right side of (16) is the achievable rate of the primary link under HIs when the spectrum resource is used by the PT only, i.e., no reflection from the BD.

Proof. Please refer to Appendix A. ■

Remark 2. Theorem 1 indicates that in the mutualistic cooperative AmBC network under HIs, even though the AmBC link brings both multipath diversity and hardware distortion noise to the primary link, the rate of the primary link can be still improved. That is, the existence of HIs does not destroy the mutual benefit between the AmBC and primary links. In particular, letting $\kappa_p = \kappa_r = 0$, Theorem 1 also verifies that the mutual benefit exists in the ideal hardware case. We note that the existence of mutual benefit in the ideal hardware case was also proven in [15], where the assumption that $c_s(i)$ follows the complex Gaussian distribution and the approximation under high signal-noise-ratio (SNR) were adopted, however, in our work, we have not made any special assumptions on the distribution of $c_s(i)$ and also not used any approximations. Thus, our proposed Theorem 1 is more general and rigorous compared to the existing one [15].

Although we provide expressions to calculate \mathcal{C}_p and its upper bound, the form of (8) is not closed and (14) is tight only at $P_0 \rightarrow \infty$. The upper bound in (14) does not hold at low or moderate transmit power. Accordingly, it is required to derive a closed-form expression that approximates \mathcal{C}_p closely at different transmit power levels. To this end, Proposition 1 is provided.

Proposition 1. By assuming that $c_s(i)$ follows the symmetric complex Gaussian distribution with zero mean and unit variance, we can approximate \mathcal{C}_p as

$$\mathcal{C}_p = \begin{cases} B_w \log_2 \left(\frac{b+b\kappa+\sigma^2}{b\kappa+\sigma^2} \right) - \frac{B_w}{\ln 2} \exp \left(\frac{b+b\kappa+\sigma^2}{a\kappa+a} \right) \text{Ei} \left(-\frac{b+b\kappa+\sigma^2}{a\kappa+a} \right) \\ \quad + \frac{B_w}{\ln 2} \exp \left(\frac{b\kappa+\sigma^2}{a\kappa} \right) \text{Ei} \left(-\frac{b\kappa+\sigma^2}{a\kappa} \right), \text{ if } \kappa > 0 \\ B_w \log_2 \left(\frac{b+\sigma^2}{\sigma^2} \right) - \frac{B_w}{\ln 2} \exp \left(\frac{b+\sigma^2}{a} \right) \text{Ei} \left(-\frac{b+\sigma^2}{a} \right), \text{ if } \kappa = 0 \end{cases}, \quad (17)$$

where $a = P_0 h \beta g$, $b = P_0 f$, and $\text{Ei}(\cdot)$ is the exponential integral.

Proof. Please refer to Appendix B. ■

Remark 3. By comparing (17) with the right side of (16), one can see that the rate gains of the primary link in the cases of HIs and ideal hardware are $\frac{B_w}{\ln 2} \exp \left(\frac{b\kappa+\sigma^2}{a\kappa} \right) \text{Ei} \left(-\frac{b\kappa+\sigma^2}{a\kappa} \right) - \frac{B_w}{\ln 2} \exp \left(\frac{b+b\kappa+\sigma^2}{a\kappa+a} \right) \text{Ei} \left(-\frac{b+b\kappa+\sigma^2}{a\kappa+a} \right)$ and $-\frac{B_w}{\ln 2} \exp \left(\frac{b+\sigma^2}{a} \right) \text{Ei} \left(-\frac{b+\sigma^2}{a} \right)$, respectively. It can also be inferred that the HIs degrade the rate gain, as $-\frac{B_w}{\ln 2} \exp \left(\frac{b+\sigma^2}{a} \right) \text{Ei} \left(-\frac{b+\sigma^2}{a} \right) > \frac{B_w}{\ln 2} \exp \left(\frac{b\kappa+\sigma^2}{a\kappa} \right) \times \text{Ei} \left(-\frac{b\kappa+\sigma^2}{a\kappa} \right) - \frac{B_w}{\ln 2} \exp \left(\frac{b+b\kappa+\sigma^2}{a\kappa+a} \right) \text{Ei} \left(-\frac{b+b\kappa+\sigma^2}{a\kappa+a} \right)$ holds at $\kappa > 0$. This indicates that although the existence of HIs does not destroy the mutual benefit between the primary and AmBC links, the harmful impacts on the rate gain exist, i.e., a larger HI level brings a smaller rate gain.

IV. RATE MAXIMIZATION

In this section, we solve two optimization problems to maximize the weighted sum rate of all links for a mutualistic cooperative AmBC network with a single AmBC link or with multiple AmBC links, respectively, while considering HIs. Different from the sum rate, the weighted sum rate not only considers the total transmission rate of the primary link and the AmBC link, but also allows for different priorities in allocating wireless resources to the primary link and the AmBC link. Particularly, when the weight factor for each link is the same, the weighted sum rate reduces the sum rate.

A. Single AmBC Link

From Section II-A, we can see that the transmit power of PT and the BD's power reflection coefficient have significant impacts on the rates of both the primary and AmBC links. This motivates us to jointly optimize these two variables to boost the achievable performance in what follows. Towards this end, we formulate a problem to maximize the weighted sum of \mathcal{C}_p and \mathcal{C}_s , while satisfying the energy-causality constraint for the BD, i.e.,

$$\mathcal{P}_0 : \max_{\beta, P_0} \theta \mathcal{C}_p + (1 - \theta) \mathcal{C}_s \quad (18a)$$

$$\text{s.t. } E_{\text{BD}} \geq P_c, \quad (18b)$$

$$0 \leq \beta \leq 1, \quad (18c)$$

$$0 < \mathbb{E} [|y_{\text{PT}}(n)|^2] \leq P_0^{\max}. \quad (18d)$$

In \mathcal{P}_0 , θ is the weight factor, (18b) is to ensure that the harvested power of the BD is always larger than the circuit consumption power P_c , (18c) and (18d) constrain the value range of the power reflection coefficient and the PT's transmit power, respectively.

Clearly, \mathcal{P}_0 is non-convex due to the following factors. On the one hand, P_0 is coupled with β in both the objective function and constraint (18b). On the other hand, the nonlinear fractional function with respect to the optimization variable is included in the objective function. To decouple the two optimization variables, we provide Proposition 2 as follows.

Proposition 2. The optimization goal of \mathcal{P}_0 is reached when the PT adopts the maximum transmit power, i.e., $P_0^* = \frac{P_0^{\max}}{1+\kappa_p^2}$.

Proof. Please refer to Appendix C. ■

Using Proposition 2, the original problem \mathcal{P}_0 can be simplified as

$$\mathcal{P}_1 : \max_{\beta} \theta \mathbb{E}_{c_s(i)} \left[\log_2 \left(1 + \frac{P_0^* h \beta g |c_s(i)|^2 + P_0^* f}{P_0^* (h \beta g |c_s(i)|^2 + f) \kappa + \sigma^2} \right) \right] \\ + \frac{1-\theta}{L} \log_2 \left(1 + \frac{L \beta h g P_0^*}{P_0^* (\beta h g + f) \kappa + \sigma^2} \right) \quad (19a)$$

$$\text{s.t. } 0 \leq \beta \leq 1 - \frac{\varphi^{-1}(P_c)}{h P_0^* (1 + \kappa_p^2)}, \quad (19b)$$

where constraint (19b) is derived from constraints (18b) and (18c). In particular, using the non-decreasing function $\varphi(\cdot)$, constraint (18b) can be rewritten as $\beta \leq 1 - \frac{\varphi^{-1}(P_c)}{h P_0^* (1 + \kappa_p^2)}$. Combining it with constraint (18c), we obtain constraint (19b). One observation from (19b) is that the feasible region of \mathcal{P}_1 is empty if $\frac{\varphi^{-1}(P_c)}{h P_0^* (1 + \kappa_p^2)} \geq 1$. Physically speaking, $\frac{\varphi^{-1}(P_c)}{h P_0^* (1 + \kappa_p^2)} \geq 1$ indicates that the harvested power is not sufficient enough to sustain the backscatter operation.

In what follows, we present a proposition to determine the optimal power reflection coefficient of \mathcal{P}_1 .

Proposition 3. The power reflection coefficient to maximize the weighted sum of \mathcal{C}_p and \mathcal{C}_s equals $1 - \frac{\varphi^{-1}(P_c)}{h P_0^* (1 + \kappa_p^2)}$, i.e., $\beta^* = 1 - \frac{\varphi^{-1}(P_c)}{h P_0^* (1 + \kappa_p^2)}$.

Proof. Please refer to Appendix D. ■

Combining propositions 2 and 3, we can rewrite β^* as

$$\beta^* = 1 - \frac{\varphi^{-1}(P_c)}{h P_0^{\max}}. \quad (20)$$

Remark 4. Observing (20) and Propositions 2, we can obtain the following interesting results. One is that the HI parameters and the channel power gain of both the primary and AmBC links have no impacts on the optimal power reflection coefficient. This indicates that the optimal power reflection coefficient is robust to the HI parameters. The other is that the optimal PT's transmit power is only determined by the HI parameters of the PT. In other words, the optimal PT's transmit power is free of the HI parameters of the PR, the power reflection coefficient and the channel power gains of all links. Accordingly, a priori knowledge of the HI parameter

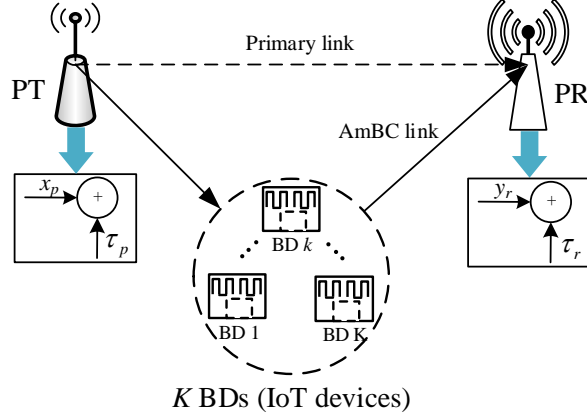


Fig. 2. Mutualistic cooperative AmBC network with multiple AmBC links.

associated with the PR and the channel power gain of both the primary and AmBC links do not be required for resource allocation in our considered network.

B. Multiple AmBC Links

In this subsection, we consider a mutualistic cooperative AmBC network with multiple BDs and formulate a problem to jointly optimize the time allocation, the transmit power of PT, and the power reflection coefficient so as to maximize the sum of weighted rate of the considered network. Subsequently we propose an iterative algorithm to solve the formulated problem.

1) *Problem Formulation and Analysis:* As shown in Fig. 2, the considered network is composed of one PT, one PR, and K BDs. In order to avoid the co-channel among BDs, the duration of an entire transmission is divided into K subslots and a TDMA scheme is adopted for BDs, where in one subslot, only one BD is allowed to backscatter its information to the PR while the other BDs operate in the energy harvesting mode. In other words, for the subslot t_k , $k = 1, 2, \dots, K$, the k -th BD works in the backscatter mode while the other BDs harvest energy from the PT's signal. Accordingly, based on the results of Section II-B, for t_k , the rate of the primary link and the k -th AmBC link can be written as, respectively,

$$\mathcal{C}_p^{t_k} = t_k \mathbb{E}_{c_s^k(i)} \left[B_w \log_2 \left(1 + \frac{P_0 h_k \beta_k g_k |c_s^k(i)|^2 + P_0 f}{P_0 (h_k \beta_k g_k |c_s^k(i)|^2 + f) \kappa + \sigma^2} \right) \right], \quad (21)$$

$$\mathcal{C}_s^{t_k} = \frac{B_w t_k}{L} \log_2 \left(1 + \frac{L \beta_k h_k g_k P_0}{P_0 (\beta_k h_k g_k + f) \kappa + \sigma^2} \right), \quad (22)$$

where h_k , g_k , and β_k are the channel power gains of the k -th BD-PT link, the k -th BD-PR link (also termed as k -th AmBC link), and the power reflection coefficient of the k -th BD within t_k , respectively.

For the k -th BD, the harvested energy in one transmission block can be written as

$$E_{\text{BD}}^k = \varphi \left((1 - \beta_k) h_k P_0 (1 + \kappa_p^2) \right) t_k + \varphi \left(h_k P_0 (1 + \kappa_p^2) \right) \sum_{i=1, i \neq k}^K t_i. \quad (23)$$

Accordingly, by considering the energy-causality constraint of each BD in each transmission block, the optimization problem to maximize the sum of weighted rate for the considered network with multiple BDs is formulated as

$$\mathcal{P}_2 : \max_{t_k, \beta_k, P_0} \sum_{k=1}^K \theta_k \mathcal{C}_s^{t_k} + \left(1 - \sum_{k=1}^K \theta_k \right) \sum_{k=1}^K \mathcal{C}_p^{t_k} \quad (24a)$$

$$\text{s.t.} \quad \sum_{k=1}^K t_k = 1, \quad (24b)$$

$$0 \leq \beta_k \leq 1, \forall k, \quad (24c)$$

$$E_{\text{BD}}^k \geq P_c t_k, \forall k, \quad (24d)$$

$$\mathcal{C}_s^{t_k} \geq R_{\min, k}, \forall k, (18d), \quad (24e)$$

where θ_k is the weight factor and satisfies $\sum_{k=1}^K \theta_k < 1$, (24e) represents the QoS constraint for each AmBC link and $R_{\min, k}$ denotes the minimum required rate for the k -th BD.

Compared to \mathcal{P}_0 , \mathcal{P}_2 is more complex and also non-convex as it includes more optimization variables and the coupled variables, i.e, t_k , β_k , and P_0 , in the objective function (24a) and the constraints (24d) and (24e). In order to decouple these optimization variables and transform \mathcal{P}_2 into a more tractable one, we first determine the optimal PT's transmit power P_0 . Similar to the

proof of proposition 2, it is easy to obtain $P_0^* = \frac{P_0^{\max}}{1+\kappa_p^2}$. Thereby, \mathcal{P}_2 is equivalent to

$$\begin{aligned} \mathcal{P}_3 : \max_{t_k, \beta_k} & \sum_{k=1}^K \frac{\theta_k t_k B_w}{L} \log_2 \left(1 + \frac{L \beta_k h_k g_k P_0^*}{P_0^* (\beta_k h_k g_k + f) \kappa + \sigma^2} \right) + \left(1 - \sum_{k=1}^K \theta_k \right) \\ & \times \sum_{k=1}^K t_k \mathbb{E}_{c_s^k(i)} \left[B_w \log_2 \left(1 + \frac{P_0^* h_k \beta_k g_k |c_s^k(i)|^2 + P_0^* f}{P_0^* (h_k \beta_k g_k |c_s^k(i)|^2 + f) \kappa + \sigma^2} \right) \right] \end{aligned} \quad (25a)$$

$$\text{s.t. (24b), (24c),} \quad (25b)$$

$$\varphi \left((1 - \beta_k) h_k P_0^* (1 + \kappa_p^2) \right) t_k + \varphi \left(h_k P_0^* (1 + \kappa_p^2) \right) \sum_{i=1, i \neq k}^K t_i \geq P_c t_k, \forall k, \quad (25c)$$

$$\frac{B_w t_k}{L} \log_2 \left(1 + \frac{L \beta_k h_k g_k P_0^*}{P_0^* (\beta_k h_k g_k + f) \kappa + \sigma^2} \right) \geq R_{\min, k}, \forall k. \quad (25d)$$

Although \mathcal{P}_3 is more tractable than \mathcal{P}_2 , it is still non-convex. The non-convexity of \mathcal{P}_3 arises from the objective function (25a) and the constraints (25c) and (25d). In particular, both the objective function and the left term of (25d) are non-convex, since they include coupled variables and the SINR is a typical nonlinear fractional term. If we consider an ideal hardware case for resource allocation, i.e., $\kappa = 0$, the SINR in the objective function would be affine. That is to say, to make the considered network more realistic, we need to devise an efficient approach to tackle the non-linear fractional term. Another difficulty is that t_k and β_k are coupled in the left term of (25c) and the non-linear energy harvesting model makes (25c) more complex and challenging. In addition, due to the non-decreasing feature of the non-linear energy harvesting model, $\varphi(\cdot)$ is a quasi-concave function and its convexity cannot be determined in generally. Therefore, we have to face the difficulties in solving the optimization problems caused by the non-linear energy harvesting model.

2) *Problem Transformation:* In order to transform \mathcal{P}_3 into a tractable form and solve the transformed one by using efficient convex optimization tools, we introduce several transformations for problem \mathcal{P}_3 in what follows.

In order to transform the objective function (25a) and the QoS constraint (25d) into concave functions, we introduce an auxiliary variable to decouple the optimization variables t_k and β_k

for each k . Specifically, let $\varepsilon_k = t_k \beta_k$ and substitute $\beta_k = \frac{\varepsilon_k}{t_k}$ into \mathcal{P}_3 , we have

$$\begin{aligned} \mathcal{P}_4 : \max_{t_k, \varepsilon_k} \quad & \sum_{k=1}^K \frac{B_w \theta_k t_k}{L} \log_2 \left(1 + \frac{P_0^* L h_k g_k \frac{\varepsilon_k}{t_k}}{P_0^* h_k g_k \kappa \frac{\varepsilon_k}{t_k} + P_0^* f \kappa + \sigma^2} \right) + \left(1 - \sum_{k=1}^K \theta_k \right) \\ & \times \sum_{k=1}^K \mathbb{E}_{c_s^k(i)} \left[B_w t_k \log_2 \left(1 + \frac{P_0^* h_k g_k |c_s^k(i)|^2 \frac{\varepsilon_k}{t_k} + P_0^* f}{P_0^* h_k \frac{\varepsilon_k}{t_k} g_k |c_s^k(i)|^2 \kappa + P_0^* f \kappa + \sigma^2} \right) \right], \end{aligned} \quad (26a)$$

$$\text{s.t. } 0 \leq \varepsilon_k \leq t_k, \forall k, \quad (24b), \quad (26b)$$

$$\varphi \left(\left(1 - \frac{\varepsilon_k}{t_k} \right) h_k P_0^* (1 + \kappa_p^2) \right) t_k + \varphi (h_k P_0^* (1 + \kappa_p^2)) \sum_{i=1, i \neq k}^K t_i \geq P_c t_k, \forall k, \quad (26c)$$

$$\frac{B_w t_k}{L} \log_2 \left(1 + \frac{P_0^* L h_k g_k \frac{\varepsilon_k}{t_k}}{P_0^* h_k g_k \kappa \frac{\varepsilon_k}{t_k} + P_0^* f \kappa + \sigma^2} \right) \geq R_{\min, k}, \forall k. \quad (26d)$$

Proposition 4. The objective function (26a) is a jointly concave function with respect to t_k and ε_k .

Proof. Please refer to Appendix E.

Next, we examine the convexity of all the constraints of \mathcal{P}_4 . It is observed that constraint (26b) is linear and constraint (26d) can be proved to be convex by using similar ways in Proposition 4, while the convexity of constraint (26c) is still unclear due to the following reasons. First, t_k is still coupled with ε_k , which brings challenges in judging its convexity. Second, the convexity of $\varphi(\cdot)$, which depends on the specific non-linear energy harvesting model, is unclear and has a significant impact on the convexity of constraint (26c). In order to make constraint (26c) more tractable, the convexity-preserving property of a perspective function [28] is leveraged. Thus, the convexity of (26c) is the same as that of the following constraint, given by

$$\varphi \left((1 - \varepsilon_k) h_k P_0^* (1 + \kappa_p^2) \right) + \varphi (h_k P_0^* (1 + \kappa_p^2)) \sum_{i=1, i \neq k}^K t_i \geq P_c t_k, \forall k. \quad (27)$$

Clearly, in constraint (27), all terms are linear except for $\varphi \left((1 - \varepsilon_k) h_k P_0^* (1 + \kappa_p^2) \right)$. Therefore, constraint (27) is convex if and only if the non-linear energy harvesting model $\varphi(\cdot)$ is a concave function. Motivated by this observation, in this work, we consider the non-linear energy harvesting model proposed in [29] as this model not only captures the nonlinear properties of a practical energy harvester, but also is a concave function with respect to the input power [30], making it more mathematically tractable than the other existing non-linear energy harvesting

models considered in [31]–[33]. The non-linear energy harvesting model proposed in [29] is given by

$$\varphi(x) = \frac{Ax + B}{x + C} - \frac{B}{C}, \quad (28)$$

where x is the input power, and the parameters A , B , and C are determined by fitting $\varphi(x)$ with the measured data.

By doing so, $\varphi(x)$ is a concave function with respect to x and thus constraint (25c) is convex. Therefore, \mathcal{P}_4 is a convex optimization problem and can be solved by the convex tools.

V. SIMULATIONS

In this section, computer simulations are provided to support our findings and verify the superiority and the effectiveness of the proposed schemes under the considered networks. Unless otherwise specified, the basic simulation parameters are set as follows. In particular, we set $P_0 = 3$ mW, $T = 1$ s, $B_w = 1$ MHz, $L = 128$ [15], $P_c = 10\mu\text{W}$ [2], $\kappa_p = \kappa_r = 0.1$ [26], and the noise power spectral density is set as $\sigma^2 = -120$ dBm/Hz [4]. Following [29] and [30], we set the parameters of the considered energy harvesting model as $A = 2.463$, $B = 1.635$ and $C = 0.826$.

A. Impacts of HIs on PT link's Rate

The standard channel fading model is considered here to characterize all the channels, where each channel power gain is given by the product of the small-scale fading and the large-scale fading. Let D_{ps} , D_{sr} and D_{pr} denote the distances of the PT-BD link, the BD-PR link and the PT-PR link, respectively. Denote h' , f' and g' as the small-scale fading of the PT-BD link, the BD-PR link and the PT-PR link, respectively. Accordingly, we have $h = h'D_{\text{ps}}^{-\alpha_{\text{ps}}}$, $f = f'D_{\text{sr}}^{-\alpha_{\text{sr}}}$ and $g = g'D_{\text{pr}}^{-\alpha_{\text{pr}}}$, where α_{ps} , α_{sr} and α_{pr} are the path loss exponents of the PT-BD link, the BD-PR link and the PT-PR link, respectively. Here α_{ps} , α_{sr} and α_{pr} are set as 2.7, 2.7 and 3. The BD's power reflection coefficient β is set as 0.8.

Fig. 3 shows the PT link's rate versus the transmit power of the PT under the HIs case and the ideal case. In order to illustrate the improvement of the PT link's rate caused by the

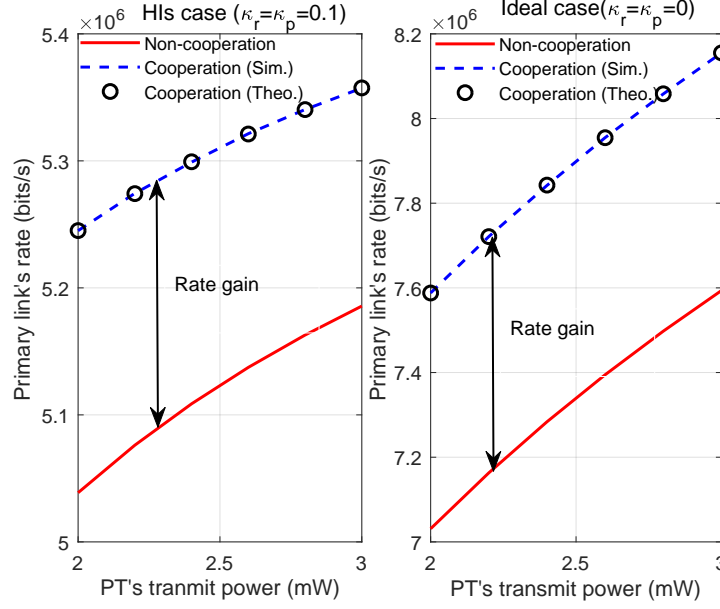


Fig. 3. The PT link's rate versus the transmit power of the PT P_0 under the HIs case and the ideal case.

BD's cooperation, we compare the PT's transmit rate under the considered network (called "Cooperation" in this figure) with the PT link's rate under the network without the BD (called "Non-cooperation" in this figure). For the PT link's rate under the considered network, we plot the simulation results and the theoretical results, respectively, where the simulation results are obtained via Monte Carlo simulations (marked by 'o') averaged over 1×10^6 realizations and the theoretical results are achieved based on the derived expression (17). It can be observed that the theoretical results match well with the simulation results, which demonstrates the correctness of (17). By comparisons, we can see that the PT link's rate under the considered network is always higher than that without the BD's cooperation in both the HIs case and the ideal case, which verifies Theorem 1, indicating that although the HI level has significant impacts on the PT link's rate, the improvement from the BD's cooperation still exists. Besides, by comparing the rate gains under the HIs case and the ideal case, we can also find that the existence of the HIs not only reduces the achievable rate at the PT, but also degrades the rate gain.

Fig. 4 plots the rates of both the primary and AmBC links versus PT's transmit power under the HIs with $\kappa_p = \kappa_r = 0.1$. The upper-bound rates of the primary and AmBC links are calculated

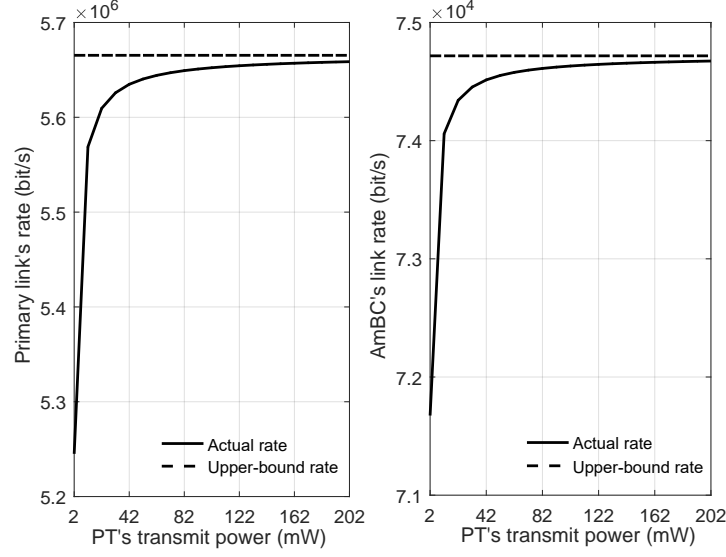


Fig. 4. The rate of both PT and AmBC links versus the transmit power.

by (14) and (15), respectively. One can see that the rates of both the primary and AmBC links under the HIs are strictly lower than the upper-bound ones. On the contrary, (12) and (13) show that in the ideal hardware case, i.e., $\kappa = \kappa_p = \kappa_r = 0$, the rates of both links increase with the PT's transmit power without an upper bound. The above observations confirm that HIs will lead to a rate ceiling for both the primary and AmBC links. This is because the HIs introduce a distortion noise whose average power is proportional to the PT's transmit power, leading to an upper-bound SINR for decoding the primary and AmBC signals, as expected in (6) and (10).

Fig. 5 illustrates the impacts of the HI levels on the PT link's rate. Here we set the values of κ_r and κ_p are the same and vary from 0 to 0.2. The reason to consider a small value for HI parameters is that the 3GPP has suggested the range of the HI level from 0.08 to 0.175 [25]. One observation is that the simulation results with the BD's cooperation (marked by 'o') always match well with the theoretical results via (17), indicating the correctness of theoretical derivations. Another observation is that the scope of the primary link's rate decreases first and then increase under the Non-cooperation or the Cooperation. This is because the primary link's

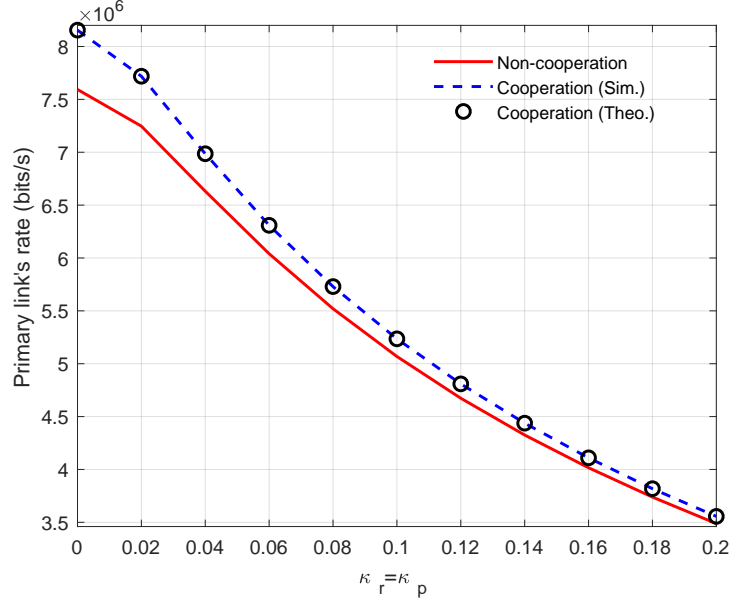


Fig. 5. The impacts of the HI levels on the PT link's rate.

rate⁵ is a non-convex with respect with respect to κ_r or κ_p . Besides, we can see that the PT link's rate with/without the BD's cooperation decrease when the HI levels increase, since the existence of the HIs degrades the achievable rate at the PT and the larger the HI levels are, the smaller the PT link's rate is. Also, the rate gain from BD's cooperation always exists no matter what the HI level is and a larger HI level brings a smaller rate gain.

B. Rate Maximization with A Single AmBC Link

Fig. 6 plots the weighted sum rate of the system versus the maximum allowed transmit power of the PT P_0^{\max} . We set $\theta = 0.2$, $B_w = 1$ MHz, and P_0^{\max} varies from 2 mW to 10 mW. Note that the optimal transmit power of the PT and the optimal power reflection coefficient of the BD under the proposed scheme are obtained by following Proposition 2 and Proposition 3. In order to demonstrate the superiority of the proposed scheme, we compare the performance of

⁵The primary link's rate is a convex function with respect to κ . However, $\kappa = \kappa_r^2 + \kappa_p^2 + \kappa_r^2 \kappa_p^2$ in our paper, and it can be proven that second derivative of the primary link's rate over κ_r or κ_p is smaller than zero first and then larger than zero as κ_r or κ_p increases.

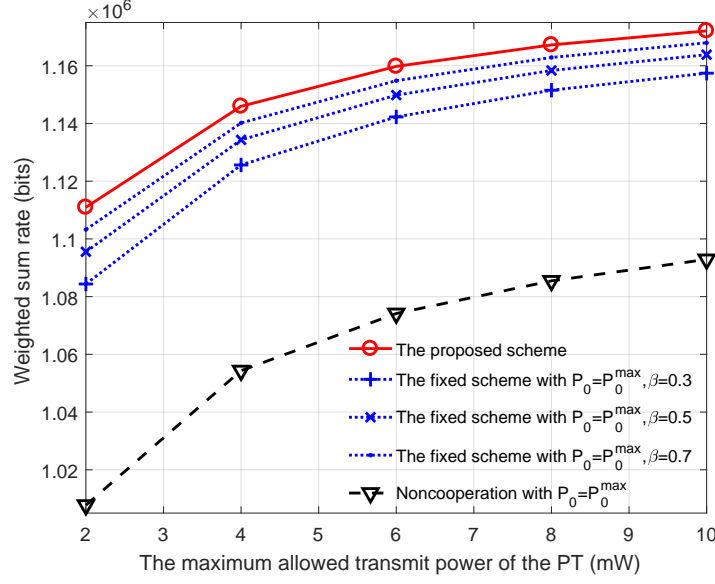


Fig. 6. The weighted sum rate of the system versus the maximum allowed transmit power of the PT.

the proposed scheme with that under the fixed scheme and non-cooperation. Specifically, for the fixed scheme, both the transmit power of the PT P_0 and the power reflection coefficient of the BD β are fixed, where P_0 is set as P_0^{\max} and β is set as 0.3, 0.5 and 0.7, respectively. For non-cooperation, P_0 is fixed as P_0^{\max} . It can be observed that with the increasing of P_0^{\max} , the weighted sum rate of the system increases since a larger P_0^{\max} brings higher PT link's rate and BD's rate, resulting in larger weighted sum rate. By comparisons, we can also see that the proposed scheme outperforms the other schemes in terms of weighted sum rate, which further illustrates the advantage of the cooperation between the PT and the BD.

C. Weighted Sum Rate Maximization with Multiple AmBC Links

In this subsection, we set $K = 4$, $P_0^{\max} = 5$ mW, $R_{\min,1} = R_{\min,2} = R_{\min,3} = R_{\min,4} = R_{\min} = 10$ kbits, $\theta_1 = \theta_2 = 0.1$ and $\theta_3 = \theta_4 = 0.2$. Let $D_{ps,k}$ and $D_{sr,k}$ denote the distance from the k -th BD to the PT and the PR, respectively. We set $D_{ps,1} = 5$ m, $D_{ps,2} = 6$ m, $D_{ps,3} = 7$ m, $D_{ps,4} = 6.5$ m, $D_{sr,1} = 11.5$ m, $D_{sr,2} = 11$ m, $D_{sr,3} = 9.5$ m, $D_{sr,4} = 10$ m and $D_{pr} = 16$ m.

Fig. 7 shows the weighted sum rate of the system versus the maximum allowed transmit power of the PT P_0^{\max} . In order to demonstrate the advantage of the proposed scheme, we compare the

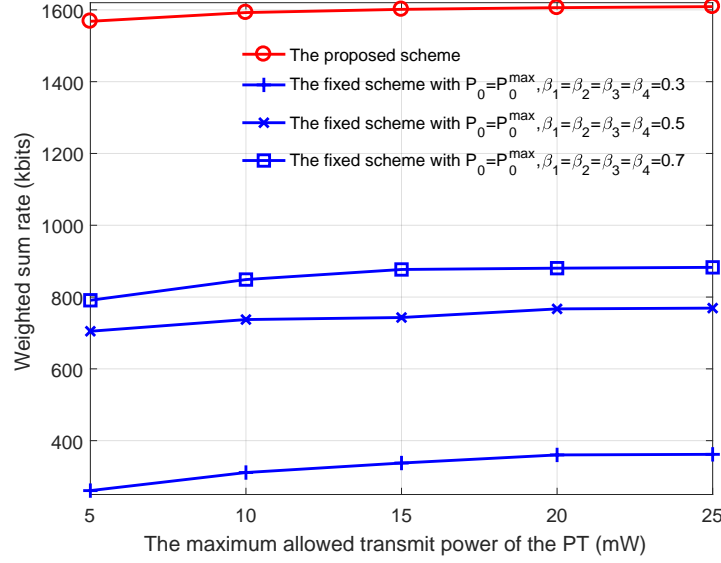


Fig. 7. The weighted sum rate of the system versus the maximum allowed transmit power of the PT.

performance of the proposed scheme with that under the fixed scheme. For the fixed scheme, the transmit power of the PT is fixed as P_0^{\max} and the backscattering time allocated for each BD is the same. The power reflection coefficient of each BD is the same and is set as 0.3, 0.5 and 0.7, respectively. It can be observed that the weighted sum rate of the system increases as P_0^{\max} increases and the proposed scheme is superior to the fixed scheme in terms of the weighted sum rate. This is because the proposed scheme provides more flexibilities to utilize resources efficiently.

Fig. 8 shows the weighted sum rate of the system versus the minimum required rate for each BD R_{\min} , where R_{\min} varies from 4 kbits to 20 kbits. It can be observed that the weighted sum rate under both the proposed scheme and the fixed schemes decreases with the increasing of R_{\min} , since a larger R_{\min} means a higher QoS requirement for each BD and more resources will be allocated to the BDs with worse channels, degrading the weighted sum rate of the system. By comparisons, we can find that the proposed scheme can achieve the highest rate, illustrating the advantage of the proposed scheme.

Fig. 9 plots the impacts of the HI levels on the weighted sum rate of the system, where the values of κ_r and κ_p are same and vary from 0.1 to 0.2. It can be observed that as the HI levels

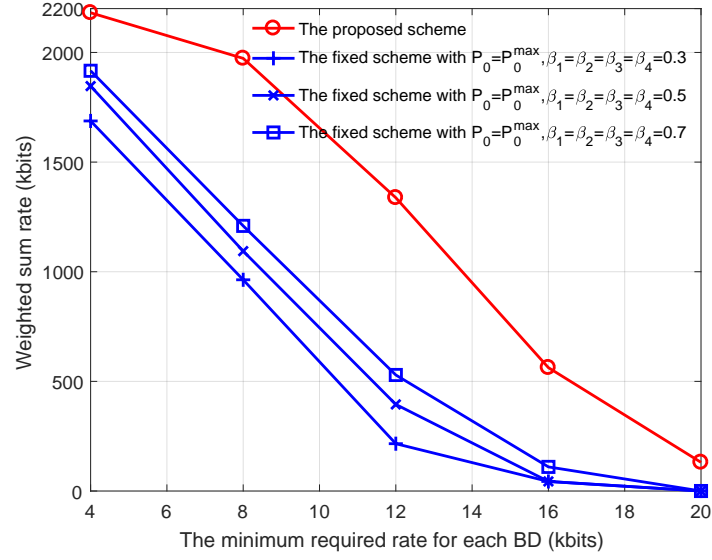


Fig. 8. The weighted sum rate of the system versus the minimum required rate for each BD.

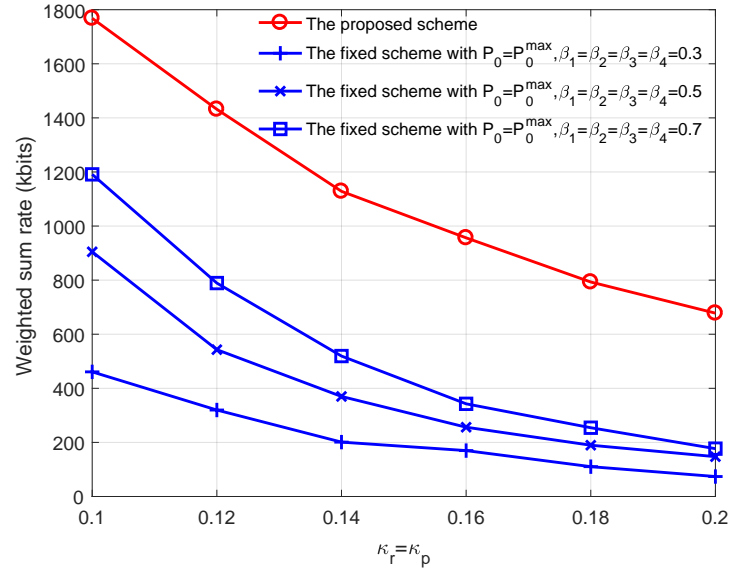


Fig. 9. The weighted sum rate of the system versus the HI levels.

increase, the weighted sum rate of the system will decrease. This is because with the increase of HI levels, the power of the distortion noise increases and thus this reduces the PT link's rate and the BD's rate. Besides, compared to the fixed scheme, where the PT's transmit power equals the optimal one while all the power reflection coefficients are fixed instead of the optimal value, we can also see that the proposed scheme can achieve a higher rate. This indicates that the value of power reflection coefficients significantly affects the achievable rates of both the primary and AmBC links.

VI. CONCLUSIONS

In this paper, we have studied the impacts of HIs and the weighted sum-rate maximization problem in the mutualistic cooperative AmBC network. We have proven that under HIs, the rates of both primary and AmBC links decrease and there exist rate ceilings for both the primary and AmBC links. We have validated that the HIs do not destroy the mutualism relationship between the AmBC link and the primary link, and have also derived closed-form expressions for both the primary and AmBC links under the assumption that the BD's message follows a symmetric complex Gaussian distribution. Two resource allocation schemes have been proposed to maximize the weighted sum rate of all links for the mutualistic cooperative AmBC network with a single AmBC link or with multiple AmBC links, respectively. In particular, the optimal solutions to the single AmBC link were derived in the closed form, while the optimal solutions to the multiple AmBC links were obtained by using convex tools to solve an equivalent convex problem. Simulation results have validated our derived results and shown that our proposed schemes achieve a higher weighted sum rate than the benchmark schemes.

APPENDIX A

Let define the following function, i.e., $\phi(x) = \frac{P_0 h \beta g x + P_0 f}{P_0 (h \beta g x + f) \kappa^2 + \sigma^2}$. Taking the first derivative of $\phi(x)$ with respect to x , we have

$$\phi'(x) = \frac{P_0^2 h \beta g \sigma^2}{(P_0 (h \beta g x + f) \kappa^2 + \sigma^2)^2} \quad (\text{A.1})$$

It is clear from (A.1) that $\phi(x)$ increases with x at $x \geq 0$. Thus, we have

$$\begin{cases} \log_2 \left(1 + \frac{P_0 h \beta g |c_s(i)|^2 + P_0 f}{P_0 (h \beta g |c_s(i)|^2 + f) \kappa^2 + \sigma^2} \right) > \log_2 \left(1 + \frac{P_0 f}{P_0 f \kappa^2 + \sigma^2} \right), & \text{if } |c_s(i)|^2 > 0, \\ \log_2 \left(1 + \frac{P_0 h \beta g |c_s(i)|^2 + P_0 f}{P_0 (h \beta g |c_s(i)|^2 + f) \kappa^2 + \sigma^2} \right) = \log_2 \left(1 + \frac{P_0 f}{P_0 f \kappa^2 + \sigma^2} \right), & \text{if } |c_s(i)|^2 = 0. \end{cases} \quad (\text{A.2})$$

In what follows, we examine the value of $|c_s(i)|^2$. In modulation schemes, different values of $c_s(i)$ are mapped to different information. If $|c_s(i)|^2 = 0$ holds for all i , BD cannot modulate its information to the PT's signal and the achievable rate of BD equals zero. Therefore, in order to achieve the information transmission of the AmBC link, $|c_s(i)|^2 = 0$ cannot be always satisfied for any given i . Combining this fact, $|c_s(i)|^2 \geq 0$ and (A.2), we reach the following result, given as

$$\begin{aligned} \mathcal{C}_p &= \mathbb{E}_{c_s(i)} \left[B_w \log_2 \left(1 + \frac{P_0 h \beta g |c_s(i)|^2 + P_0 f}{P_0 (h \beta g |c_s(i)|^2 + f) \kappa^2 + \sigma^2} \right) \right] \\ &> \mathbb{E}_{c_s(i)} \left[B_w \log_2 \left(1 + \frac{P_0 f}{P_0 f \kappa^2 + \sigma^2} \right) \right] \\ &= B_w \log_2 \left(1 + \frac{P_0 f}{P_0 f \kappa^2 + \sigma^2} \right). \end{aligned} \quad (\text{A.3})$$

Theorem 1 can be proven by (A.3) and the proof is complete.

APPENDIX B

As $c_s(i)$ obeys a standard symmetric complex Gaussian distribution, the distribution of $|c_s(i)|^2$ is an exponential function with parameter one. Based on this, (8) can be rewritten as

$$\begin{aligned} \mathcal{C}_p &= \mathbb{E}_{c_s(i)} [R_p(c_s(i))] \\ &\stackrel{x=|c_s(i)|^2}{=} \int_0^\infty B_w \log_2 \left(1 + \frac{ax + b}{a\kappa x + b\kappa + \sigma^2} \right) \exp(-x) dx \\ &= \underbrace{\int_0^\infty B_w \log_2 ((a\kappa + a)x + b + b\kappa + \sigma^2) \exp(-x) dx}_{\Delta_1} \\ &\quad - \underbrace{\int_0^\infty B_w \log_2 (a\kappa x + b\kappa + \sigma^2) \exp(-x) dx}_{\Delta_2}, \end{aligned} \quad (\text{B.1})$$

where $a = P_0 h \beta g$ and $b = P_0 f$. Using integration by parts, we have

$$\begin{aligned}
\Delta_1 &= -B_w \log_2 (b + b\kappa + \sigma^2 + (a\kappa + a)x) \exp(-x) \Big|_0^\infty \\
&\quad + \frac{B_w (a\kappa + a)}{\ln 2} \int_0^\infty \frac{\exp(-x)}{b + b\kappa + \sigma^2 + (a\kappa + a)x} dx \\
&= B_w \log_2 (b + b\kappa + \sigma^2) + \frac{B_w}{\ln 2} \int_0^\infty \frac{e^{-x}}{\frac{b+b\kappa+\sigma^2}{a\kappa+a} + x} dx \\
&= B_w \log_2 (b + b\kappa + \sigma^2) - \frac{B_w}{\ln 2} \exp\left(\frac{b + b\kappa + \sigma^2}{a\kappa + a}\right) \text{Ei}\left(-\frac{b + b\kappa + \sigma^2}{a\kappa + a}\right), \tag{B.2}
\end{aligned}$$

where the last equality is derived from $\int_0^\infty \frac{\exp(-\mu x) dx}{x + \beta} = -\exp(\mu\beta) \text{Ei}(-\mu\beta)$, as shown in eq.(3.352.4) of [34].

Similar as above, Δ_2 can be calculated as

$$\begin{aligned}
\Delta_2 &= -B_w \log_2 (a\kappa x + b\kappa + \sigma^2) e^{-x} \Big|_0^\infty + \frac{B_w}{\ln 2} \int_0^\infty \frac{e^{-x}}{a\kappa x + b\kappa + \sigma^2} dx \\
&= \begin{cases} B_w \log_2 (b\kappa + \sigma^2) + \frac{B_w}{a\kappa \ln 2} \int_0^\infty \frac{e^{-x}}{x + \frac{b\kappa + \sigma^2}{a\kappa}} dx, & \text{if } \kappa > 0 \\ B_w \log_2 (b\kappa + \sigma^2), & \text{if } \kappa = 0 \end{cases} \\
&= B_w \log_2 (b\kappa + \sigma^2) - \begin{cases} \frac{B_w}{\ln 2} \exp\left(\frac{b\kappa + \sigma^2}{a\kappa}\right) \text{Ei}\left(-\frac{b\kappa + \sigma^2}{a\kappa}\right), & \text{if } \kappa > 0 \\ 0, & \text{if } \kappa = 0 \end{cases}. \tag{B.3}
\end{aligned}$$

Substituting (B.2) and (B.3) into (B.1), we can reach (17) and the proof is complete.

APPENDIX C

From (8) and (11), it is not hard to infer that the monotonicities of \mathcal{C}_p and \mathcal{C}_s are the same as $\gamma_{x_p}(c_s(i)) = \frac{P_0 h \beta g |c_s(i)|^2 + P_0 f}{P_0 (h \beta g |c_s(i)|^2 + f) \kappa + \sigma^2}$ and $\gamma_{c_s} = \frac{L \beta h g P_0}{P_0 (\beta h g + f) \kappa + \sigma^2}$, respectively. Dividing the numerator and denominator by P_0 , we have $\gamma_{x_p}(c_s(i)) = \frac{h \beta g |c_s(i)|^2 + f}{(h \beta g |c_s(i)|^2 + f) \kappa + \sigma^2 / P_0}$ and $\gamma_{c_s} = \frac{L \beta h g}{(\beta h g + f) \kappa + \sigma^2 / P_0}$, indicating that both $\gamma_{x_p}(c_s(i))$ and γ_{c_s} increase with P_0 . Accordingly, the objective function increases with the growth of P_0 . Combining all the constraints of problem \mathcal{P}_0 , it can be inferred that the upper bound of P_0 is $\frac{P_0^{\max}}{1 + \kappa_p^2}$. Accordingly, allowing P_0 equal $\frac{P_0^{\max}}{1 + \kappa_p^2}$ can maximize the weighted sum of \mathcal{C}_p and \mathcal{C}_s , and Proposition 2 is proven.

APPENDIX D

For ease of analysis, let $\phi(\beta) = \theta\phi_1(\beta) + \frac{1-\theta}{L}\phi_2(\beta)$ denote the objective function of \mathcal{P}_1 , where $\phi_1(\beta) = \mathbb{E}_{c_s(i)} \left[B_w \log_2 \left(1 + \frac{P_0^* h \beta g |c_s(i)|^2 + P_0^* f}{P_0^* (h \beta g |c_s(i)|^2 + f) \kappa + \sigma^2} \right) \right]$ and $\phi_2(\beta) = B_w \log_2 \left(1 + \frac{L \beta h g P_0^*}{P_0^* (\beta h g + f) \kappa + \sigma^2} \right)$. Subsequently, we will prove that both $\phi_1(\beta)$ and $\phi_2(\beta)$ are two increasing functions with respect to β .

The monotonicity of $\phi_1(\beta)$: Since the expectation operator does not affect the monotonicity and the logarithmic function $\log_2(1+x)$ increases with x , the monotonicity of $\phi_1(\beta)$ is the same as $\frac{P_0^* h \beta g |c_s(i)|^2 + P_0^* f}{P_0^* (h \beta g |c_s(i)|^2 + f) \kappa + \sigma^2}$. Through some convenient mathematical calculations, we have

$$\frac{P_0^* h \beta g |c_s(i)|^2 + P_0^* f}{P_0^* (h \beta g |c_s(i)|^2 + f) \kappa + \sigma^2} = \frac{1}{\kappa} \left(1 - \frac{\sigma^2}{P_0^* (h \beta g |c_s(i)|^2 + f) \kappa + \sigma^2} \right). \quad (\text{D.1})$$

The above equation (D.1) indicates that $\frac{P_0^* h \beta g |c_s(i)|^2 + P_0^* f}{P_0^* (h \beta g |c_s(i)|^2 + f) \kappa + \sigma^2}$ increases with β . Thus, the $\phi_1(\beta)$ is an increasing function.

Similar as above, it is not hard to prove that $\phi_2(\beta)$ increases with β . Based on the above results, we can show that the objective function of \mathcal{P}_1 also increases with β . Combining it with constraint (19b), proposition 3 can be proven.

APPENDIX E

The convexity of (26a) is determined by the following two terms, given by,

$$\Delta_1 = t_k \log_2 \left(1 + \frac{P_0^* L h_k g_k \kappa \frac{\varepsilon_k}{t_k}}{P_0^* h_k g_k \kappa \frac{\varepsilon_k}{t_k} + P_0^* f \kappa + \sigma^2} \right), \quad (\text{E.1})$$

$$\Delta_2 = \mathbb{E}_{c_s^k(i)} \left[t_k \log_2 \left(1 + \frac{P_0^* h_k g_k |c_s^k(i)|^2 \frac{\varepsilon_k}{t_k} + P_0^* f}{P_0^* h_k \frac{\varepsilon_k}{t_k} g_k |c_s^k(i)|^2 \kappa + P_0^* f \kappa + \sigma^2} \right) \right]. \quad (\text{E.2})$$

If both Δ_1 and Δ_2 are jointly concave functions with respect to t_k and ε_k , Proposition 4 can be proven.

The convexity of Δ_1 : As Δ_1 is the perspective function of $\Delta_3 = \log_2 \left(1 + \frac{P_0^* L h_k g_k \varepsilon_k}{P_0^* h_k g_k \kappa \varepsilon_k + P_0^* f \kappa + \sigma^2} \right)$ and the perspective operation preserves convexity, the convexity of Δ_1 is the same as Δ_3 that is the composition of $\phi_1(x) = \log_2(1+x)$ and $\phi_2(\varepsilon_k) = \frac{P_0^* L h_k g_k \varepsilon_k}{P_0^* h_k g_k \kappa \varepsilon_k + P_0^* f \kappa + \sigma^2}$. Due to $\frac{\partial^2 \phi_2(\varepsilon_k)}{\partial \varepsilon_k^2} = -\frac{L}{\kappa} \frac{2(P_0^* h_k g_k \kappa)^2 (P_0^* f \kappa + \sigma^2)}{(P_0^* h_k g_k \kappa \varepsilon_k + P_0^* f \kappa + \sigma^2)^3} < 0$, $\phi_2(\varepsilon_k)$ is a concave function. Combining it with the fact that

$\phi_1(x)$ is concave and nondecreasing, it can be inferred that Δ_3 is a concave function according to (3.10) of [28].

The convexity of Δ_2 : Let define a function as $\Delta_4 = \mathbb{E}_{c_s^k(i)} \left[\log_2 \left(1 + \frac{P_0^* h_k g_k |c_s^k(i)|^2 \varepsilon_k + P_0^* f}{P_0^* h_k \varepsilon_k g_k |c_s^k(i)|^2 \kappa + P_0^* f \kappa + \sigma^2} \right) \right]$. Using the perspective of a function, the convexity of Δ_2 is the same as that of Δ_4 . Recall that the expectation operator preserves convexity of Δ_4 . Accordingly, Δ_2 is a concave function if and only if $\Delta_5 = \log_2 \left(1 + \frac{P_0^* h_k g_k |c_s^k(i)|^2 \varepsilon_k + P_0^* f}{P_0^* h_k \varepsilon_k g_k |c_s^k(i)|^2 \kappa + P_0^* f \kappa + \sigma^2} \right)$ is a concave function with respect to ε_k . Similar to (D.1), we have $\Delta_5 = \log_2 \left(1 + \frac{1}{\kappa} \Delta_6 \right)$, where $\Delta_6 = 1 - \frac{\sigma^2}{P_0^* h_k \varepsilon_k g_k |c_s^k(i)|^2 \kappa + P_0^* f \kappa + \sigma^2}$. Due to $\frac{\partial^2 \Delta_6}{\partial \varepsilon_k^2} < 0$, Δ_6 is a concave function on ε_k . Combining this conclusion with the fact that $\log_2(1+x)$ is concave and nondecreasing, we can say that Δ_5 is concave.

Based on the above analysis and derivations, we can prove that the objective function (26a) is concave.

REFERENCES

- [1] Y. Ye, L. Shi, X. Chu, G. Lu, and S. Sun, "Impacts of hardware impairments on mutualistic cooperative ambient backscatter communications," in *Proc. IEEE ICC*, 2022, pp. 1–6.
- [2] C. Xu, L. Yang, and P. Zhang, "Practical backscatter communication systems for battery-free internet of things: A tutorial and survey of recent research," *IEEE Signal Process. Mag.*, vol. 35, no. 5, pp. 16–27, 2018.
- [3] Y. Ye, L. Shi, X. Chu, and G. Lu, "On the outage performance of ambient backscatter communications," *IEEE Internet Things J.*, vol. 7, no. 8, pp. 7265–7278, 2020.
- [4] X. Lu, H. Jiang, D. Niyato, D. I. Kim, and Z. Han, "Wireless-powered device-to-device communications with ambient backscattering: Performance modeling and analysis," *IEEE Trans. Wireless Commun.*, vol. 17, no. 3, pp. 1528–1544, 2018.
- [5] V. Liu *et al.*, "Ambient backscatter: wireless communication out of thin air," in *Proc. ACM SIGCOMM*, 2013, p. 1216.
- [6] B. Kellogg *et al.*, "Wi-Fi backscatter: Internet connectivity for RF-powered devices," in *Proc. ACM SIGCOMM*, 2014, pp. 607–618.
- [7] S. N. Daskalakis, J. Kimionis, A. Collado, G. Goussetis, M. M. Tentzeris, and A. Georgiadis, "Ambient backscatterers using FM broadcasting for low cost and low power wireless applications," *IEEE Trans. Microw. Theory Techn.*, vol. 65, no. 12, pp. 5251–5262, 2017.
- [8] C. Liu, Z. Wei, D. W. K. Ng, J. Yuan, and Y.-C. Liang, "Deep transfer learning for signal detection in ambient backscatter communications," *IEEE Trans. Wireless Commun.*, vol. 20, no. 3, pp. 1624–1638, 2021.
- [9] Q. Tao, C. Zhong, X. Chen, H. Lin, and Z. Zhang, "Optimal detection for ambient backscatter communication systems with multiantenna reader under complex gaussian illuminator," *IEEE Internet Things J.*, vol. 7, no. 12, pp. 11 371–11 383, 2020.
- [10] G. Yang, Y.-C. Liang, R. Zhang, and Y. Pei, "Modulation in the air: Backscatter communication over ambient OFDM carrier," *IEEE Trans. Commun.*, vol. 66, no. 3, pp. 1219–1233, 2018.

- [11] Y.-C. Liang, Q. Zhang, E. G. Larsson, and G. Y. Li, "Symbiotic radio: Cognitive backscattering communications for future wireless networks," *IEEE Trans. Cogn. Commun. Netw.*, vol. 6, no. 4, pp. 1242–1255, 2020.
- [12] H. Guo, Y.-C. Liang, R. Long, and Q. Zhang, "Cooperative ambient backscatter system: A symbiotic radio paradigm for passive IoT," *IEEE Wireless Commun. Lett.*, vol. 8, no. 4, pp. 1191–1194, 2019.
- [13] X. Kang, Y.-C. Liang, and J. Yang, "Riding on the primary: A new spectrum sharing paradigm for wireless-powered IoT devices," in *Proc. IEEE ICC*, 2017, pp. 1–6.
- [14] G. Yang, Q. Zhang, and Y.-C. Liang, "Cooperative ambient backscatter communications for green internet-of-things," *IEEE Internet Things J.*, vol. 5, no. 2, pp. 1116–1130, 2018.
- [15] R. Long, Y.-C. Liang, H. Guo, G. Yang, and R. Zhang, "Symbiotic radio: A new communication paradigm for passive internet of things," *IEEE Internet Things J.*, vol. 7, no. 2, pp. 1350–1363, 2020.
- [16] Z. Chu, W. Hao, P. Xiao, M. Khalily, and R. Tafazolli, "Resource allocations for symbiotic radio with finite blocklength backscatter link," *IEEE Internet Things J.*, vol. 7, no. 9, pp. 8192–8207, 2020.
- [17] X. Chen, H. V. Cheng, K. Shen, A. Liu, and M.-J. Zhao, "Stochastic transceiver optimization in multi-tags symbiotic radio systems," *IEEE Internet Things J.*, vol. 7, no. 9, pp. 9144–9157, 2020.
- [18] R. Long, H. Guo, and Y.-C. Liang, "Symbiotic radio with full-duplex backscatter devices," in *Proc. IEEE ICC*, 2019, pp. 1–6.
- [19] H. Yang, Y. Ye, K. Liang, and X. Chu, "Energy efficiency maximization for symbiotic radio networks with multiple backscatter devices," *IEEE Open J. Commun. Soc.*, vol. 2, pp. 1431–1444, 2021.
- [20] Z. Ding, "Harvesting devices' heterogeneous energy profiles and QoS requirements in IoT: WPT-NOMA vs BAC-NOMA," *IEEE Trans. Commun.*, vol. 69, no. 5, pp. 2837–2850, 2021.
- [21] Q. Zhang, L. Zhang, Y.-C. Liang, and P. Y. Kam, "Backscatter-NOMA: An integrated system of cellular and internet-of-things networks," in *Proc. IEEE ICC*, 2019, pp. 1–6.
- [22] S. Zhou, W. Xu, K. Wang, C. Pan, M.-S. Alouini, and A. Nallanathan, "Ergodic rate analysis of cooperative ambient backscatter communication," *IEEE Wireless Commun. Lett.*, vol. 8, no. 6, pp. 1679–1682, 2019.
- [23] E. Costa and S. Pupolin, "M-QAM-OFDM system performance in the presence of a nonlinear amplifier and phase noise," *IEEE Trans. Commun.*, vol. 50, no. 3, pp. 462–472, 2002.
- [24] Z. Liu, G. Lu, Y. Ye, and X. Chu, "System outage probability of PS-SWIPT enabled two-way AF relaying with hardware impairments," *IEEE Trans. Veh. Technol.*, vol. 69, no. 11, pp. 13 532–13 545, 2020.
- [25] E. Björnson, J. Hoydis, M. Kountouris, and M. Debbah, "Massive MIMO systems with non-ideal hardware: Energy efficiency, estimation, and capacity limits," *IEEE Trans. Inf. Theory*, vol. 60, no. 11, pp. 7112–7139, 2014.
- [26] X. Li, M. Zhao, M. Zeng, S. Mumtaz, V. G. Menon, Z. Ding, and O. A. Dobre, "Hardware impaired ambient backscatter NOMA systems: Reliability and security," *IEEE Trans. Commun.*, vol. 69, no. 4, pp. 2723–2736, 2021.
- [27] G. Wang, F. Gao, R. Fan, and C. Tellambura, "Ambient backscatter communication systems: Detection and performance analysis," *IEEE Trans. Commun.*, vol. 64, no. 11, pp. 4836–4846, 2016.
- [28] S. Boyd, *Convex optimization*. Cambridge, UK: Cambridge University Press, 2004.
- [29] Y. Chen, N. Zhao, and M. Alouini, "Wireless energy harvesting using signals from multiple fading channels," *IEEE Trans. Commun.*, vol. 65, no. 11, pp. 5027–5039, 2017.

- [30] Y. Ye, L. Shi, X. Chu, and G. Lu, "Throughput fairness guarantee in wireless powered backscatter communications with HTT," *IEEE Wireless Commun. Lett.*, vol. 10, no. 3, pp. 449–453, 2021.
- [31] S. Wang, M. Xia, K. Huang, and Y.-C. Wu, "Wirelessly powered two-way communication with nonlinear energy harvesting model: Rate regions under fixed and mobile relay," *IEEE Trans. Wireless Commun.*, vol. 16, no. 12, pp. 8190–8204, 2017.
- [32] L. Shi, Y. Ye, R. Q. Hu, and H. Zhang, "Energy efficiency maximization for SWIPT enabled two-way DF relaying," *IEEE Signal Process. Lett.*, vol. 26, no. 5, pp. 755–759, 2019.
- [33] E. Boshkovska, D. W. K. Ng, N. Zlatanov, and R. Schober, "Practical non-linear energy harvesting model and resource allocation for SWIPT systems," *IEEE Commun. Lett.*, vol. 19, no. 12, pp. 2082–2085, 2015.
- [34] I. S. Gradshteyn and I. M. Ryzhik, *Table of integrals, series, and products*, 7th ed. New York, NY, USA: Academic press, 2007.